Materials Research. 2025; 28: e20250447
DOI: https://doi.org/10.1590/1980-5373-MR-2025-0447

The Influence of Niobium Addition on the Mechanical Properties and Microstructure of High-Strength Low-Alloy Steel Processed Through a Conventional Rolling Mill

Camila de Brito Ferreira[a*] **,** ***Leonardo Contri Campanelli***[a] **,** ***Anibal de Andrade Mendes Filho***[b] **,**
Gisele Maria Leite Dalmonico[c] **,** ***Danieli Aparecida Pereira Reis***[a]

[a]*Universidade Federal de São Paulo (UNIFESP), Instituto de Ciência e Tecnologia (ICT), São José dos Campos, SP, Brasil.*
[b]*Universidade Federal do ABC (UFABC), Centro de Engenharia, Modelagem e Ciências Sociais Aplicadas (CECS), Santo André, SP, Brasil.*
[c]*Centro Brasileiro de Pesquisas Físicas (CBPF), Rio de Janeiro, RJ, Brasil.*

Received: May 09, 2025; Revised: September 19, 2025; Accepted: October 26, 2025

The high-strength low-alloy (HSLA) steels present a challenge in balancing mechanical performance, cost and formability. The HSLA steel design involves adjusting the carbon (C) content and incorporating microalloying elements such as niobium (Nb), vanadium (V), titanium (Ti), which contribute through precipitation hardening, solid solution strengthening, and grain refinement. Nb is the primary microalloying element; it enhances tensile properties by refining the austenitic grain size during hot rolling, increasing hardness, and providing strength, usually, via Nb(C,N) or NbC precipitation. The morphology, size, and distribution of these precipitates critically impact the steel's behavior. Thermo-Mechanical Control Processing (TMCP) further enhances material properties through Nb addition. However, the effectiveness of Nb in the continuous rolling of long products requires thorough evaluation. This study addresses this issue by quantifying and correlating the effect of Nb under conditions different from those of TMCP, evaluating its effect on the grain size, tensile properties, impact energy absorption, and hardness of AISI 4320 steel following conventional rolling. The results indicate that Nb addition between 200 and 500 ppm improves the yield strength by approximately 10%, while the ultimate tensile strength increases by about 6%. The particle size distribution of the precipitates reveals unusual findings regarding the grain refinement capability of Nb.

Keywords: *HSLA; niobium, alloy composition, microstructure, mechanical properties.*

1. Introduction

The automotive industry continually strives to reduce vehicle weight without compromising passenger safety or component durability. A key route toward this goal is the use of high-strength low-alloy (HSLA) and microalloyed steels, which balance strength, ductility, and cost by incorporating small quantities of microalloying elements (e.g., Nb, V, Ti) that form carbides, nitrides, and carbonitrides to refine grain size, retard phase transformations, and strengthen the steel via precipitation hardening[1-3].

Nb, in particular, is known to suppress austenite grain growth, retard recrystallization during hot deformation, and form stable Nb(C,N) precipitates that pin grain boundaries and inhibit dynamic recrystallization[2,4]. These effects are especially exploited in thermomechanical controlled processing (TMCP), where deformation conditions are precisely controlled to optimize precipitate distribution and mechanical response[5].

However, much of the literature on Nb-microalloyed steels focuses on either TMCP routes or thermal simulations of heat-affected zones (HAZ), and there is limited information on their behavior in the as-rolled condition, especially for SAE 4320 steel. For example, Yang et al.[6] studied the influence of Nb in the coarse grain heat-affected zone (CGHAZ) using thermal simulations and found that Nb did not significantly affect prior austenite grain size, but it promoted acicular ferrite nucleation through interactions with inclusions and altered nano-inclusion precipitation. Despite its relevance, this study does not address the actual as-rolled microstructure prior to any thermal treatment.

Moreover, several works emphasize the importance of hot deformation parameters (such as strain rate and inter-pass time) in controlling microstructural evolution and precipitate behavior[7]. In conventional rolling, high strain rates ($>1000\ s^{-1}$) and short inter-pass times (<1 s) differ markedly from TMCP conditions, which may result in distinct precipitate distributions and austenite grain structures. Nonetheless, few studies explore how Nb behaves under these industrially relevant rolling conditions in medium carbon, alloyed steels such as SAE 4320.

SAE 4320 is widely used for case-hardened automotive components due to its excellent core toughness and surface hardness after carburizing. While some studies have investigated Nb's role in heat-treated or pseudo-carburized conditions[8],

*e-mail: camilabferreira@hotmail.com
Associate Editor: Hugo Sandim.
Editor-in-Chief: Luiz Antonio Pessan.

there is a lack of data on the microstructural and mechanical effects of Nb in the initial as-rolled state, which is critical because this initial condition directly influences austenite grain growth, diffusion kinetics, and precipitate behavior during subsequent heat treatments.

Therefore, this study aims to fill this gap by investigating SAE 4320 steel with and without Nb addition in its as-rolled condition. The work characterizes precipitate types, sizes, and spatial distributions, as well as austenite grain structure and mechanical properties before any thermal or carburizing treatments. By linking the early microstructural state to potential downstream performance, this study provides valuable insights into how Nb additions may be tailored to improve processing efficiency and final component performance.

2. Materials and Method

In this study, an analysis of two batches was conducted, one of which conformed to the SAE 4320 standard and the other incorporated Nb as a microalloying element. The steels were produced in an electric arc furnace (EAF), followed by vacuum degassing (VD) and continuous casting. The chemical compositions of the steels are presented in Table 1. The values for C and S were obtained using the combustion and inert gas fusion technique with a LECO CS 230 according to ASTM E1019[9]. For the other elements, an ARL Model 4460 optical emission spectrometer was used in accordance with ASTM E415[10]. Samples were taken during the continuous casting process. The elements listed in the table correspond to those present in the final steel composition, including both intentionally added and unintentionally incorporated elements.

The billets produced in the casting process had a nominal size of 240 × 240 mm. In the first step, the billets underwent rolling to achieve dimensions of 155 × 155 mm. This first reduction step was performed under conventional rolling conditions, with the sole purpose of dimensional adjustment. Therefore, the rolling temperature at this stage was not controlled or recorded, as it had no intended influence on the final microstructure or mechanical properties. The billets were then ground and subsequently rolled into round bars with a final dimension of 57.15 mm. Both rolling processes are classified as conventional.

For the final rolling process, the billets were reheated at approximately 1055 °C (average value), with a standard deviation of 8 °C, for approximately 2 hours. These temperatures correspond to measurements taken by the first pyrometer immediately after the billets exited the heating furnace. This reheating temperature reflects typical industrial practice, selected to ensure a balance between plastic deformation, surface quality, and process stability. Additional rolling parameters such as strain rate and reduction per pass were consistent with conventional industrial practices, although specific values are not reported herein due to proprietary process constraints. After rolling, the bars were cooled in air.

Thermodynamic modeling of precipitate formation was performed using Thermo-Calc software to predict the temperatures of precipitate formation and the volume fractions of the constituent phases under equilibrium conditions. The chemical compositions of the studied steels were used as input parameters. Simulations were conducted using the TCFE-7 database to model precipitation sequences during cooling over a temperature range of approximately 600 °C to 1500 °C. This allowed the identification and quantification of precipitates such as Nb(C,N), AlN, and TiN. Additionally, critical phase transformation temperatures were evaluated using JMatPro software.

The microstructure was evaluated in specimens with transverse orientations in the core region of the bar. Microstructure revelation was achieved through etching with a 2% Nital reagent, facilitating the identification of the present phases. Images were captured using a Tescan Scanning Electron Microscope (SEM), model VEGA 3. To evaluate the austenitic grain size, samples from the middle radius of a randomly selected section of the bar were analyzed. The testing methodology followed ASTM E112-13[11] standard for direct hardening steels (885 °C for 1 hour). The analysis was performed using Picral etching and the austenitic grain size was determined using an Olympus BX60 microscope, along with the Leica QGrain application from Leica Microsystems Imaging Solutions Ltd based on 15 fields.

To evaluate the distribution of precipitates in the samples, transmission electron microscopy (TEM) analyses were conducted in the cross-section. TEM analyses were performed using a JEOL JEM-2100 microscope with a LaB6 gun, operating at 200 kV and a magnification of 100,000x considering 3 replicates of each sample. Precipitate characterization was performed on carbon replicas via SEM using a JEOL JEM7100F-LV microscope in the STEM-in-SEM scanning transmission electron microscopy transmission mode. Particles were then measured to determine their equivalent circular diameter (ECD) considering 50 fields per steel. The crystal structure was analyzed using selected area electron diffraction (SAED) for selected precipitates.

Six samples, each approximately 300 mm in length, were randomly taken from the bars for mechanical testing. Five of these samples were used for tensile tests on the cores, performed according to ASTM A370-22[12], resulting in five independent replicates. The tests were conducted on a Kratos ECC universal testing machine with a 50,000 kgf capacity, equipped with a contact extensometer for direct measurement

Table 1. Chemical compositions of the steels used in this study and the SAE specification (wt.%). S, Al, Nb, N and Ti values are given in ppm (*).

Steel	C	Mn	P	Si	Cr	Ni	Mo	S*	Al*	Nb*	N*	Ti
SAE 4320	0.17-0.22	0.45-0.65	0.030 max.	0.15-0.35	0.40-0.60	1.65-2.00	0.20-0.30	400 max.	-	-	-	-
4320 STD	0.18	0.57	0.017	0.23	0.53	1.74	0.24	300 max.	200-300	100 max.	100-200	20 max.
4320 Nb(1)	0.20	0.59	0.017	0.23	0.53	1.70	0.21	300 max.	200-300	200-500	100-200	20 max.

of elongation to fracture. Hydraulic grips were used to prevent specimen slippage during testing, and the TRClv61430l system handled data control and analysis. Another sample was used for the hardness and impact tests. The impact test was performed in accordance with ASTM E23-18 utilizing a Heckert impact machine with a capacity of 294 J[13]. The HB measurement was carried out with a durometer from Shimadzu Seisakusho LTD, using a ϕ10 mm ball indenter with a maximum capacity of 3,000 kgf, according to ASTM E10-18[14]. The hardness analysis was performed in triplicate on the middle radius of the cross-section of the bar sample, and the impact test was performed in five replicates on test specimens from the same region of the sample.

A statistical assessment of mechanical properties was performed using Student's t-test. A significance level (α) of 0.05 was adopted, indicating the probability of rejecting the null hypothesis (H_0), which states that the mean values of the analyzed characteristics are identical across different steels. The p-value obtained for each case determines whether H_0 can be rejected. If the p-value is greater than α, H_0 is not rejected, indicating no significant difference among the steels for that property. If the p-value is less than or equal to α, H_0 is rejected. The confidence interval used was set at 95%.

3. Results and Discussion

3.1. Microstructure characterization

Figure 1 shows SEM micrographs of the cross-section of 4320 STD and 4320 Nb(1) steels after conventional rolling and air cooling. Both steels exhibit a microstructure predominantly composed of bainite (indicated by B) with some regions of ferrite (indicated by A). While Nb addition is generally expected to refine the microstructure by promoting finer bainite and grain boundary pinning through Nb(C,N) precipitates, in this study the observed microstructural differences were subtle. This limited effect is attributed to the processing conditions, which did not allow full Nb dissolution and fine precipitation, resulting in the expected refinement effect of Nb not being clearly observed at this stage.

Based on the chemical compositions of the steels, an analysis of the precipitates present was performed while considering thermodynamic equilibrium aspects. For this purpose, graphs were constructed using Thermo-Calc software and are shown in Figure 2.

The thermodynamic simulations were performed to estimate the equilibrium precipitation temperatures of key phases such as TiN, Nb(C,N), and AlN. The distinct curves observed for TiN and AlN reflect their different thermodynamic stabilities: TiN forms at significantly higher temperatures due to titanium's strong affinity for nitrogen and its low solubility in austenite, while AlN precipitates at lower temperatures as a result of aluminum's comparatively weaker nitride-forming tendency. These behaviors affect when and how each precipitate forms during steel processing and solidification[15].

Although 4320 STD steel was not intentionally microalloyed with elements such as Nb or Ti, chemical analysis confirmed their presence in measurable amounts. In particular, Ti readily forms stable TiN precipitates during solidification, even in small concentrations. These particles may affect austenitic grain growth during reheating and subsequent rolling. Thermodynamic predictions suggest that the reheating temperature (1055 °C) may not be sufficient for complete Nb dissolution. This hypothesis will be assessed later.

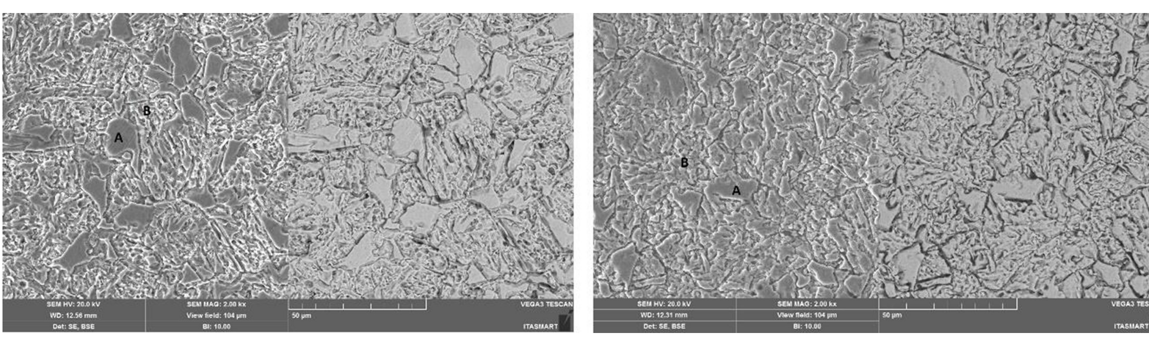

Figure 1. Cross-section microstructure using 2% Nital etching after rolling for 4320 STD steel (left) and 4320 Nb(1) steel (right) obtained by SEM.

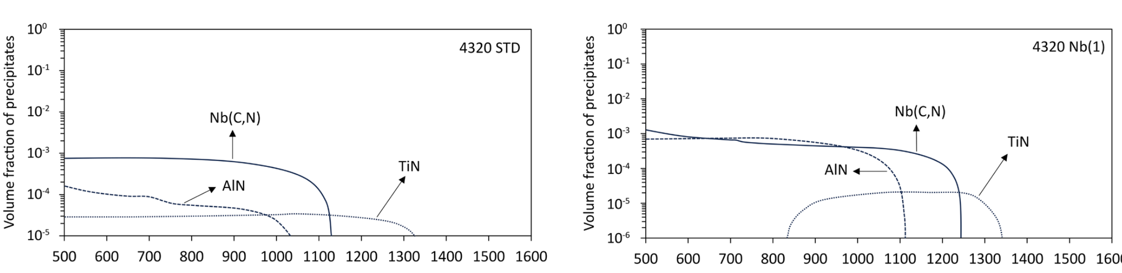

Figure 2. Thermodynamic simulation of precipitate formation using Thermo-Calc software for the studied steels.

Notably, the data obtained through the software represent thermodynamic equilibrium conditions, and under industrial processing conditions (such as those in the rolling mill), they fall outside both thermodynamic and kinetic equilibrium. As the rolling temperature was the same for both steels, it was not sufficient for all of the contained and intentionally added Nb to be completely dissolved and precipitated in the form of Nb(C,N) for the 4320 Nb(1) steel, because the temperature should be higher than 1200 °C. Based on the values used in this study, it is possible to observe that most of the precipitate formed during the steel solidification process, which can lead to coarser precipitates.

Although these results do not fully represent the industrial conditions to which steels are subjected, the thermodynamic simulations performed prior to processing serve as predictive tools to understand the potential behavior of Nb in the steel matrix under ideal equilibrium conditions[16]. These simulations, combined with experimental observations of grain size and precipitate distribution, allow us to infer whether Nb would dissolve adequately during rolling to precipitate and become finely dispersed, thus acting as a grain refiner.

However, it is important to highlight that the actual hot rolling conditions employed (temperature of 1055 °C and heating time of 2 hours) were insufficient to achieve complete dissolution and fine precipitation of Nb(C,N), as confirmed by both thermodynamic predictions and microstructural analyses. Consequently, the expected grain refinement effect of Nb was not observed in the present study. This outcome suggests that, under the given processing parameters, Nb precipitates remain relatively coarse, limiting their ability to effectively pin grain boundaries and refine the austenite grain size[17]. Future studies incorporating processing conditions closer to industrial hot rolling parameters, such as higher reheating temperatures (>1200 °C) and optimized holding times, are necessary to fully evaluate the potential grain refining role of Nb in these steels.

3.2. Precipitate characterization

Figure 3 shows TEM images and the nanostructures in 4320 STD steel, including the size distribution of precipitates and the corresponding selected area electron diffraction (SAED) patterns.

The precipitates in the steel exhibited a cubic morphology, as shown in Figures 3(a) and 3(b). As mentioned earlier, although Ti was not intentionally added during steel design, its presence was confirmed via chemical analysis, and the formation of second-phase particles containing Ti was observed. Selected area electron diffraction (SAED) confirmed the presence of TiN precipitates, as shown in Figure 3(c). TiN is known for its high thermal stability and resistance to coarsening, characteristics that enable it to contribute to austenite grain boundary pinning[18]. Figure 3(d) and Figure 3(e) show bright-field and dark-field images of the TiN precipitate, respectively, which were obtained using (200) reflection. In the high-resolution image, it is possible to measure the interplanar distance of 2.123Å corresponding to the (200) plane of the TiN precipitate in Figure 3(f) and Figure 3(g). It is evident from these images that TiN grains are around 20 nm in size. The size distribution of the precipitate in the steel without Nb is not very homogeneous and is mainly less than 25 nm in size, according to the histogram presented in Figure 3(h).

The TEM images in Figure 4 present the nanostructures in 4320 Nb(1) steel, including the size distribution of the precipitates. The precipitates from 4320 Nb(1) steel exhibit round contours instead of cubic shapes and are larger (Figure 4(a) and (b)). The morphology of precipitates can influence their mechanical properties. The presence of cubic precipitates can generate stress concentrators that increase the probability of fractures. Furthermore, edges hinder the movement of dislocations and can contribute to greater hardness and yield strength. Circular precipitates result in a lower probability of stress concentrators and consequently greater ductility. Although no microalloying element was added to the 4320 STD steel, this study sought to highlight the typical precipitates present in both steels and compare how they affect the other properties. The SAED patterns were identified, as shown in Figure 4(c). An analysis of the bright-field image in Figure 4(d) and the dark-field image indicates that most precipitated particles of NbC were verified by using the (200) reflection in SAED. The precipitate with a size around 200 nm shown in Figure 4(e) is oriented close to the [001] zone axis with a hexagonal crystal structure on the plane (200). According to the histogram in Figure 4(f), the highest frequency of precipitates in the 4320 Nb(1) steel is in the range of 125 to 175 nm, while that in the 4320 STD steel is less than 25 nm. In terms of chemical composition, the precipitate analyzed in the 4320 Nb(1) sample is rich in both Nb and C, while the precipitate observed in the 4320 STD steel contains several elements, with C being the most prevalent.

The distribution and size of precipitates play important roles in pinning austenite grains. While the chemical composition of precipitates is an important factor in steel design and processing control, this alone does not fully explain the effect of precipitates on steels. In automotive structural applications, larger particles primarily influence ductile fracture processes and fatigue, whereas smaller particles effectively interfere with grain boundaries and dislocations. The critical size that separates larger and smaller particles is somewhat dependent on the properties of the steel; however, in general, constituents in the micrometer range are considered larger, while nanometer-sized particles can effectively interact with dislocations and grain boundaries[19]. Our results show that the second-phase particles in microalloyed steel were not small enough to promote a pinning effect. Thus, it is important to determine whether these particles significantly impact the austenitic grain size or mechanical properties of the studied steels.

3.3. Grain size evolution

The grain size distribution plot is shown in Figure 5. The results indicate that the grain sizes for 4320 STD steel and 4320 Nb(1) steel are similar (ASTM grain size numbers of 9.6 and 10, respectively). However, the histograms reveal that 4320 Nb(1) steel exhibits lower variability in grain size, indicating a more uniform distribution. This suggests that the presence of Nb contributes to a more homogeneous grain size distribution.

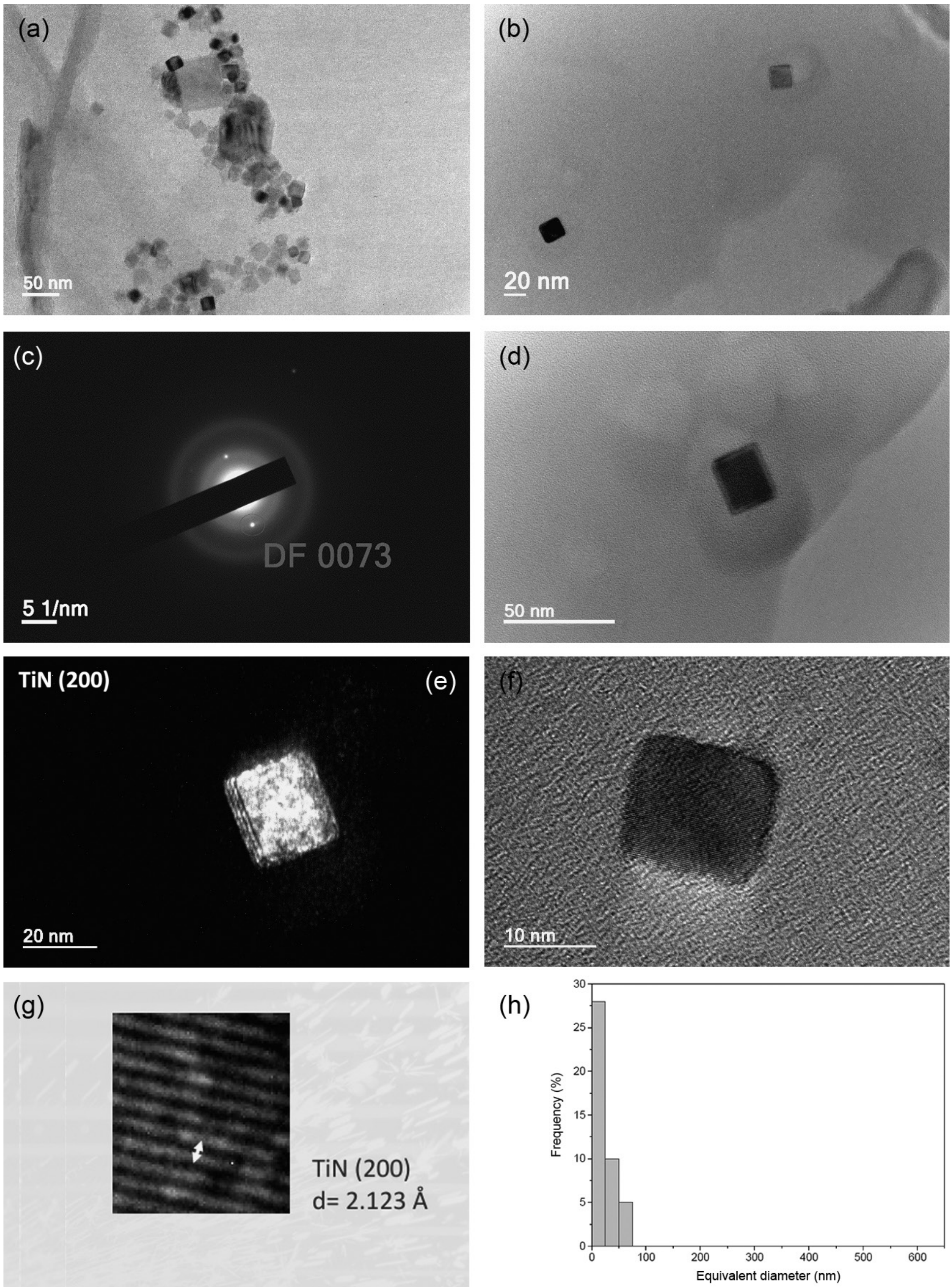

Figure 3. TEM results from the center region of 4320 STD steel: (a)-(b) precipitates in the cross-section, (c) SAED, (d) bright-field image, (e) dark-field image of the TiN precipitate using the (200) reflection, (f) high-resolution TEM image of the TiN precipitate, (g) interplanar distance analysis, and (h) size distribution of the precipitates.

This aspect is particularly relevant for carburized automotive components, where grain size uniformity plays a critical role. Several studies have demonstrated that austenite grain size has a direct influence on the fatigue performance of carburized steels. While grain size is typically controlled through chemical composition and heat treatment during later processing stages[20-23], there is limited data regarding its behavior in the as-rolled condition, which corresponds to the initial state of raw material before carburizing. In this study, we compared the austenite grain size distribution of 4320 steel with and without Nb additions. As shown in Figure 5, both steels presented similar average grain sizes (ASTM grain size numbers of 9.6 and 10, respectively). However, the Nb-containing steel exhibited lower variability in grain size, suggesting a more uniform structure even under conventional rolling conditions. This observation contributes to our understanding of how early-stage processing affects microstructural uniformity in steels intended for fatigue-critical automotive applications.

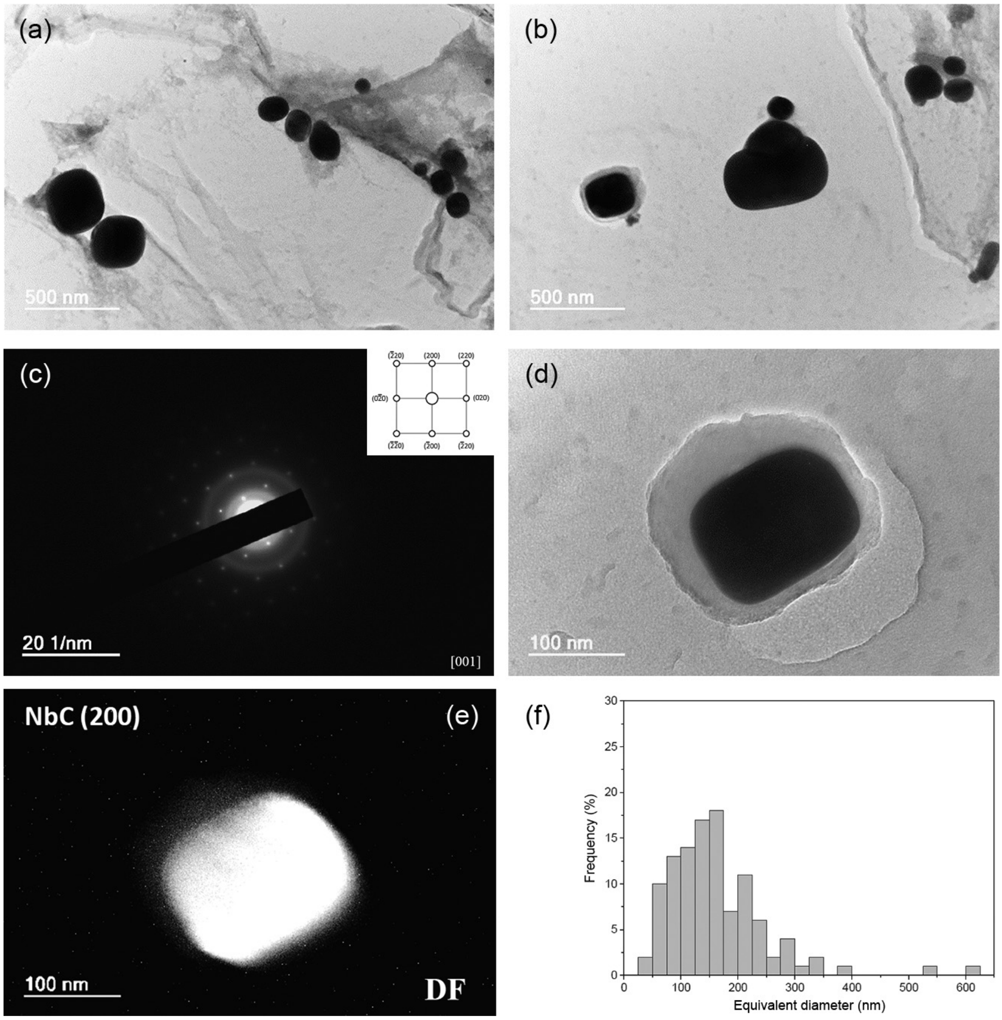

Figure 4. TEM results from the center region of 4320 Nb(1) steel: (a)-(b) precipitates in the cross-section, (c) SAED with zone axis [001], (d) bright-field image, (e) dark-field image of the NbC precipitate using the (200) reflection, and (f) size distribution of the precipitates.

This result appears to partially conflict with the literature that characterizes Nb as a grain refiner. However, it is necessary to consider that the precipitation of Nb present in the steel may have occurred in two stages: during the solidification of the steel and during the reheating of the rolling mill. The thermodynamic data show that the reheating temperature of the billets was not sufficient for the complete dissolution of Nb and its possible reprecipitation, as previously discussed. Moreover, precipitates larger than 100 nm are less effective at grain boundary pinning[19]. Therefore, although it was expected that the addition of Nb would promote grain refinement, this effect was not achieved due to the temperature and reheating time applied, which generated coarse precipitates.

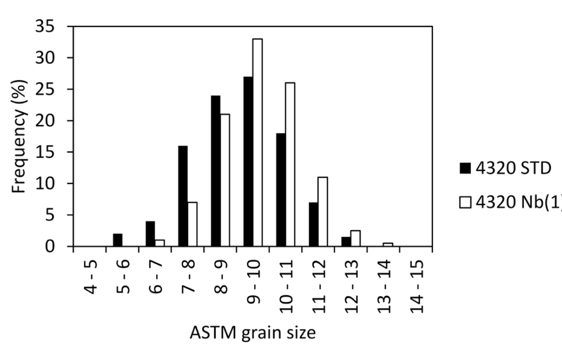

Figure 5. ASTM grain size distribution for both steels.

3.4. Mechanical properties and statistical analysis

To evaluate the mechanical characteristics, tensile properties, impact resistance, and hardness were analyzed to determine whether the addition of Nb influences these properties. A statistical assessment of these attributes was performed using Student's t-test, and the results are presented in Table 2.

The results show no significant differences between the steels regarding elongation, reduction in area, absorbed energy, and hardness, as indicated by their p-values, all of which are greater than the significance level of 0.05. In contrast, the yield strength shows a significant difference between the 4320 STD and 4320 Nb(1) steels, with a p-value of 4.00×10^{-6}.

Table 2. Mechanical properties with their respective standard deviations and p-values (obtained using Student's t-test).

Mechanical properties	4320 STD	4320 Nb(1)	P-value
YS (MPa)	474 ± 7	519 ± 5	4.00×10^{-6}
US (MPa)	746 ± 11	792 ± 18	3.00×10^{-3}
Elongation (%)	22.3 ± 0.2	22.1 ± 0.1	6.30×10^{-2}
Reduction of Area (%)	52.0 ± 0.6	52.5 ± 0.7	3.37×10^{-1}
Absorbed Energy (J)	32.9 ± 2.7	31.5 ± 1.7	3.72×10^{-1}
Hardness (HB)	231.0 ± 3.0	235.0 ± 0.5	1.83×10^{-1}

This indicates that the addition of Nb has a statistically significant effect on the yield strength, as the 4320 Nb(1) steel exhibited an improvement in this property. The same conclusion applies to ultimate tensile strength, which has a p-value of 0.003, further confirming the impact of Nb.

When analyzed under conventional rolling conditions in the as-rolled state, the moderate effect of Nb on the mechanical properties and the absence of an effect on grain refinement among the steels are consistent with the results obtained for the distribution of precipitate sizes, especially when compared with its impact under TMCP conditions. Most of the precipitates are larger than 100 nm and, as previously discussed, lose the grain pinning effect. This finding highlights the importance of analyzing the use of Nb in different processing conditions that are not addressed in the literature.

As previously demonstrated, the Nb-rich precipitates were relatively coarse and not well-dispersed, indicating limited precipitation strengthening. Therefore, the primary mechanism contributing to the observed improvements in mechanical properties is likely solid-solution strengthening. While the differences in elongation, reduction in area, absorbed energy, and hardness were not statistically significant, further investigation into Nb's effects in the case-hardened state could yield valuable insights. Examining its influence on fatigue life may reveal additional enhancements in material properties, underscoring the potential benefits of Nb in steel formulations for automotive applications.

In addition to the effects of Nb, it is important to emphasize that Ti, despite not being intentionally added during alloy design, was present in measurable amounts and led to the formation of TiN precipitates. These nanoscale (~20 nm) particles are well-known for their strong interaction with grain boundaries, contributing to grain growth inhibition and enhanced microstructural stability[18]. Although the impact of TiN may be secondary relative to Nb-containing precipitates in this study, its presence still notably influences the microstructure and mechanical properties, especially in the 4320 STD steel where Nb(C,N) precipitation was limited. From an industrial standpoint, this underscores the necessity to carefully control Ti content during steel production, as even trace amounts can affect processing costs and the final balance of mechanical properties. Thus, considering Ti effects is essential for accurate interpretation and optimization of steel behavior in practical applications.

4. Conclusion

This study evaluated the influence of Nb addition (200-500 ppm) on the microstructure and mechanical properties of 4320 steel subjected to conventional rolling and air cooling, conditions that are less explored compared to TMCP processing. The key findings are:

- The addition of Nb led to a statistically significant increase in yield strength (~10%) and ultimate tensile strength (~6%), despite the absence of notable grain size refinement.
- Both steels exhibited similar average austenitic grain sizes; however, the Nb-containing steel showed a more uniform grain size distribution.
- Microstructural analyses revealed that Nb precipitates were relatively coarse (>100 nm) under the applied thermal conditions, limiting their grain boundary pinning effectiveness and, consequently, the expected grain refinement.
- TiN precipitates, present due to trace Ti content, were observed in the nanometric range (~20 nm), influencing grain growth inhibition and microstructural stability, especially in the steel without intentional Nb addition.

These results suggest that under conventional rolling conditions, Nb's strengthening effect is primarily due to solid-solution hardening, rather than precipitation strengthening or grain refinement. Optimizing reheating temperature and holding time above 1200 °C is necessary to achieve finer Nb(C,N) precipitates and maximize their beneficial effects.

From an industrial perspective, controlling Ti content and understanding the interplay between Nb and Ti precipitates are crucial for balancing mechanical properties and processing costs. Overall, this work provides new insights into the role of Nb under conventional rolling, offering guidance for tailoring processing parameters to improve the performance of 4320 steel in automotive applications.

5. Acknowledgments

This study was conducted at Gerdau S.A. in Pindamonhangaba, SP, in partnership with the Laboratory of Mechanical Behavior of Metals at the Federal University of São Paulo and with the Federal University of ABC. The authors would like to thank FINEP, FAPESP, CAPES, and CNPq for their financial support.

6. References

1. Zhang D, Liu G, Zhang K, Sun X, Liang X, Yong Q. Effect of Nb microalloying on microstructure evolution and mechanical properties in low carbon medium manganese steel. Mater Sci Eng A. 2021;824:141813. http://doi.org/10.1016/j.msea.2021.141813.
2. Sun L, Liu X, Xu X, Lei S, Li H, Zhai Q. Review on niobium application in microalloyed steel. J Iron Steel Res Int. 2022;29(10):1513-25. http://doi.org/10.1007/s42243-022-00789-1.

3. Gao WL, Leng Y, Fu DF, Teng J. Effects of niobium and heat treatment on microstructure and mechanical properties of low carbon cast steels. Mater Des. 2016;105:114-23. http://doi.org/10.1016/j.matdes.2016.05.057.
4. Irvine KJ, Pickering FB, Gladman T. Grainrefined CMn steels. J Iron Steel Inst. 1967;205:161-82.
5. Pereda B, RodriguezIbabe JM, Lopez B. Modeling of austenite evolution during hot rolling of mediumHigh C long products. In: International Conference on Advances in Metallurgy of Long and Forged Products; 2021 July 12-14; Virtual Conference. Proceedings. Association of Iron and Steel Technology; 2022.
6. Yang Y, Jia X, Ma Y, Wang P, Zhu F. Effect of Nb on inclusions and phase transformation in simulated high heat input coarse-grain HAZ of Nb/Ti low carbon microalloyed steel. Mater Charact. 2022;189:111947. http://doi.org/10.1016/j.matchar.2022.111966.
7. De A, Dutta B. Thermomechanical processing of advanced highstrength steels. In: Haldar A, Suwas S, Bhattacharjee D, editors. Microstructure evolution in metal forming processes. Cambridge: Woodhead Publishing; 2012. p. 295322.
8. An X, Cao W, Zhang X, Yu J. Suppress Austenite Grain Coarsening by Nb Alloying in High–Temperature–Pseudo–Carburized Bearing Steel. Materials. 2024;17(12):2962. https://doi.org/10.3390/ma17122962.
9. ASTM: American Society for Testing and Materials. ASTM E101918: standard test methods for determination of carbon, sulfur, nitrogen, and oxygen in steel, iron, nickel, and cobalt alloys by various combustion and inert gas fusion techniques. West Conshohocken: ASTM International; 2018.
10. ASTM: American Society for Testing and Materials. ASTM E41521: standard test method for analysis of carbon and lowalloy steel by spark atomic emission spectrometry. West Conshohocken: ASTM International; 2021.
11. ASTM: American Society for Testing and Materials. ASTM E11213: standard test methods for determining average grain size. West Conshohocken: ASTM International; 2013.
12. ASTM: American Society for Testing and Materials. ASTM A37022: standard test methods and definitions for mechanical testing of steel products. West Conshohocken: ASTM International; 2022.
13. ASTM: American Society for Testing and Materials. ASTM E2318: standard test methods for notched bar impact testing of metallic materials. West Conshohocken: ASTM International; 2018.
14. ASTM: American Society for Testing and Materials. ASTM E1018: standard test method for brinell hardness of metallic materials. West Conshohocken: ASTM International; 2018.
15. Chang LZ, Shi XF, Zhou L, Wang JJ. Thermodynamic calculation of microalloy precipitation in austenite region for FeCNAlTiNb steel. Adv Mat Res. 2012;476478:205-11. http://doi.org/10.4028/www.scientific.net/AMR.476-478.205.
16. Yamini AS. Influence of microalloying elements (Ti, Nb) and nitrogen concentrations on precipitation of pipeline steels: A thermodynamic approach. Eng Rep. 2021;3(7):e12337. https://doi.org/10.1002/eng2.12337.
17. Rakshe B, Patel J, Palmiere EJ. Effect of Niobium Supersaturation in Austenite on the Static Recrystallization Behavior of Carbon Structural Steels. Metall Mater Trans, A Phys Metall Mater Sci. 2022;53(8):3143-57. https://doi.org/10.1007/s11661-022-06733-y.
18. Zhu F, Wang P, Li Z, Yang Y. Effect of TiN precipitates on austenite grain growth in highstrength steel. Materials. 2022;15(9):3176. http://doi.org/10.3390/ma15093176.
19. Silva ALVC. Second phases in steel: a review of the concept, origin, and their relevance for properties. Tecnol Metal Mater Min. 2022;19:e2753. http://doi.org/10.4322/2176-1523.20222753.
20. Sanders JA. The effects of shot peening on the bending fatigue behavior of a carburized SAE 4320 [thesis]. Golden (CO): Colorado School of Mines; 1993.
21. Lee S, Seo EJ, Cryderman RL, Matlock DK, Speer JG. Effects of cold work on abnormal grain growth during simulated carburizing of AISI 4121 steel containing Nb. In: 31st ASM Heat Treating Society Conference & Exposition – Heat Treat 2021; 2021 Sep 14–16; St. Louis. Extended Abstracts. Geauga (OH): ASM International; 2021. p. 229237.
22. Matlock DK, Krauss G, Speer JG. New microalloyed steel applications for the automotive sector. Mater Sci Forum. 2005;500501:87-96. http://doi.org/10.4028/www.scientific.net/MSF.500-501.87.
23. Klinkenberg C, Trute S, Bleck W. Niobium in engineering steels for automotive applications. Steel Res Int. 2006;77(910):698-703. http://doi.org/10.1002/srin.200606450.

Data Availability

All data supporting the findings of this study have been published within the article itself.